ЖУРНАЛ ФІЗИЧНИХ ДОСЛІДЖЕНЬ
т. 23, № 3 (2019) 3702(8 с.)

JOURNAL OF PHYSICAL STUDIES
v. 23, No. 3 (2019) 3702(8 p.)

EFFECT OF STRESSES σ_5, σ_6 AND ELECTRIC FIELD E_3 ON THERMODYNAMIC CHARACTERISTICS OF GPI FERROELECTRIC

A. S. Vdovych[1], R. R. Levitskii[1], I. R. Zachek[2]
[1] *Institute for Condensed Matter Physics of the National Academy of Sciences of Ukraine*
1, Svientsitskii St., Lviv, UA–79011, Ukraine
[2] *Lviv Polytechnic National University*
12, Bandery St., Lviv, UA–79013, Ukraine
(February 11, 2019; in final form — March 19, 2019)

The model of glycine phosphite (GPI) ferroelectric, modified by taking into account the piezoelectric coupling between the ordering structure elements and the lattice strains ε_j, is used for the investigation into the effects appearing under shear stresses σ_5, σ_6 and electric field E_3. Within the framework of the two particle cluster approximation, the components of the polarization vector and the static dielectric permittivity tensor of a mechanically clamped crystal, and also their piezoelectric and thermal characteristics are calculated. The simultaneous effects of shear stress σ_5 and field E_3 as well as the effects of stress σ_6 and field E_3 on the phase transition and physical characteristics of the crystal are studied.

Key words: ferroelectrics, phase transition, dielectric permittivity, piezoelectric coefficients, shear stress effect, electric field effect.

DOI: https://doi.org/10.30970/jps.23.3702

PACS number(s): 77.22.−d, 77.22.Ch, 77.22.Ej, 77.65.−j, 77.80.Bh

I. INTRODUCTION

Investigation into the effects appearing under mechanical stress and external electric field is one of actual problems in the physics of ferroelectric materials, especially regarding the glycine phosphite crystal (GPI) that belongs to the ferroelectric compounds with hydrogen bonds [1].

Refs. [2,3] describe an experimental study of the effect of the transverse electric field E_3 on the transverse dielectric permittivity ε_{33} of GPI crystal. It is shown that the electric field E_3 decreases the phase transition temperature proportionally to E_3^2. Considerable (and increasing with the field) anomalies of the permittivity ε_{33} were revealed in the phase transition region at $E_3 \neq 0$. An explanation of the revealed effects is presented in [2–4] based on phenomenologic theory as well as within the microscopic approach using the proposed proton model of GPI. But a complete quantitative description of the experimental data was not achieved.

In [5], based on the proton model [3], a model of deformed crystal is proposed, which takes into account the piezoelectric coupling of the proton and lattice subsystems. Using this model, the effect of electric fields E_1 and E_3 on the dielectric and piezoelectric properties of GPI was investigated. The abovementioned experimental data [3] for the temperature dependence of ε_{33} in the presence of field E_3 were quantitatively correctly described.

The model of GPI [5] was generalised in [7] to the case of the reduction of symmetry in the presence of the shear strains ε_4 and ε_6. Another special case was studied: the effect of shear stresses on a GPI crystal in the absence of any electric field. It was shown that the shear stress σ_5 does not change the thermodynamic characteristics qualitatively, but the shear stresses σ_4 or σ_6 lead to the appearance of the components of a spontaneous polarization along OX and OZ axes in the ferroelectric phase, and to the appearance of a divergence at the temperature T_c in trasverse permittivities ε_{11} and ε_{33}.

In the present paper, based on model [7], we investigate the general case of a simultaneous effect of the transverse electric field E_3 and the shear stresses σ_6 and σ_6 on the phase transition and on the dielectric and piezoelectric characteristics of GPI. Also we demonstrate, how the results previously obtained in [5] are reproduced within the model generalised in [7].

II. THE MODEL OF GPI CRYSTAL

Models [5,7] consider the system of protons in GPI, localised on O–H...O bonds between the phosphite groups HPO_3, which form zigzag chains along the crystallographic c-axis of the crystal (see Fig. 1). For a better understanding of the model, only the phosphite groups are shown in the figure. Dipole moments $\mathbf{d}_{qf}(f = 1, \ldots, 4)$ are ascribed to the protons on the bonds. In the ferroelectric phase, the dipole moments compensate each other ($\mathbf{d}_{q1}$ with $\mathbf{d}_{q3}$, $\mathbf{d}_{q2}$ with $\mathbf{d}_{q4}$) in directions Z and X ($X \perp (b,c), Y \parallel b, Z \parallel c$), and simultaneously supplement each other in direction Y, creating a spontaneous polarization.

Pseudospin variables $\frac{\sigma_{q1}}{2}, \ldots, \frac{\sigma_{q4}}{2}$ describe the reorientation of the dipole moments of the base units: $\mathbf{d}_{qf} = \boldsymbol{\mu}_f \frac{\sigma_{qf}}{2}$. Mean values $\langle \frac{\sigma}{2} \rangle = \frac{1}{2}(n_a - n_b)$ are connected with the differences in the occupancy of the two possible molecular positions, n_a and n_b.

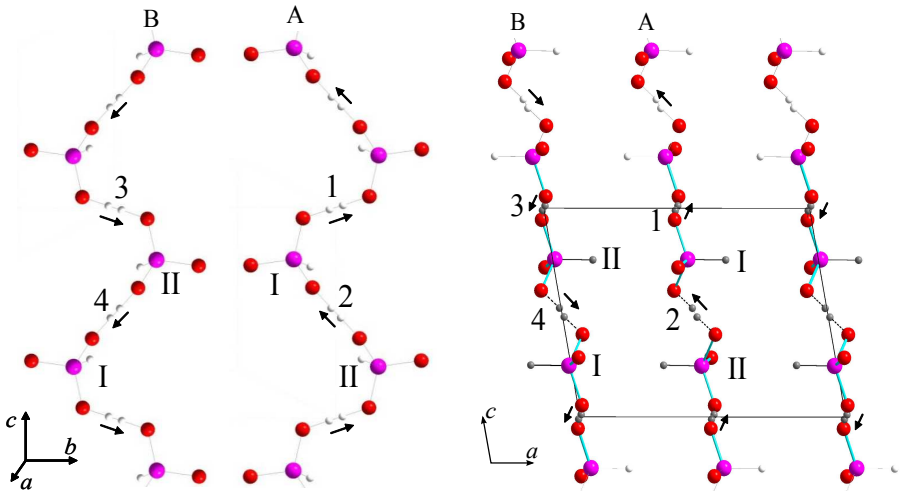

Fig. 1. Orientations of vectors $\mathbf{d}_{qf}$ in the primitive cell in ferroelectric phase [5, 7].

Hereinafter for convenience we use notations 1, 2 and 3 instead of x, y and z for components of vectors and tensors. The Hamiltonian of the proton subsystem of GPI, which takes into account the short-range and long-range interactions, and also the applied machanical stresses and electric fields E_1, E_2, E_3 along the positive directions of the Cartesian axes X, Y and Z, can be written in such a way [7]:

$$\hat{H} = NU_{\text{seed}} + \hat{H}_{\text{short}} + \hat{H}_{\text{long}} + \hat{H}_E, \tag{2.1}$$

where N is the total number of primitive cells. The term U_{seed} in (2.1) is the "seed" energy, which relates to the heavy ion sublattice and does not explicitly depend on the configuration of the proton subsystem. It includes elastic, piezolectric and dielectric parts, expressed in terms of electric fields E_i (i=1, 2, 3) and strains ε_j (j=1,...,6):

$$U_{\text{seed}} = v\Bigg(\frac{1}{2}\sum_{j,j'=1}^{6} c_{jj'}^{E0}(T)\varepsilon_j\varepsilon_{j'} - \sum_{i=1}^{3}\sum_{j=1}^{6} e_{ij}^{0}\varepsilon_j E_i - \sum_{i,i'=1}^{3}\frac{1}{2}\chi_{ii'}^{\varepsilon 0}E_iE_{i'}\Bigg). \tag{2.2}$$

Parameters $c_{jj'}^{E0}(T)$, e_{ij}^{0}, $\chi_{ii'}^{\varepsilon 0}$ are the so called "seed" elastic constants, "seed" coefficients of piezoelectric stresses and "seed" dielectric susceptibilities, respectively; v is the volume of a primitive cell. Matrices $c_{jj'}^{E0}$, e_{ij}^{0}, $\chi_{ii'}^{\varepsilon 0}$ are given by:

$$\hat{c}_{jj'}^{E0} = \begin{pmatrix} c_{11}^{E0} & c_{12}^{E0} & c_{13}^{E0} & 0 & c_{15}^{E0} & 0 \\ c_{12}^{E0} & c_{22}^{E0} & c_{23}^{E0} & 0 & c_{25}^{E0} & 0 \\ c_{13}^{E0} & c_{23}^{E0} & c_{12}^{E0} & 0 & c_{35}^{E0} & 0 \\ 0 & 0 & 0 & c_{44}^{E0} & 0 & c_{46}^{E0} \\ c_{15}^{E0} & c_{25}^{E0} & c_{35}^{E0} & 0 & c_{55}^{E0} & 0 \\ 0 & 0 & 0 & c_{46}^{E0} & 0 & c_{66}^{E0} \end{pmatrix}, \quad \hat{e}_{ij}^{0} = \begin{pmatrix} 0 & 0 & 0 & e_{14}^{0} & 0 & e_{16}^{0} \\ e_{21}^{0} & e_{22}^{0} & e_{23}^{0} & 0 & e_{25}^{0} & 0 \\ 0 & 0 & 0 & e_{34}^{0} & 0 & e_{36}^{0} \end{pmatrix}, \quad \hat{\chi}_{ii'}^{\varepsilon 0} = \begin{pmatrix} \chi_{11}^{\varepsilon 0} & 0 & \chi_{13}^{\varepsilon 0} \\ 0 & \chi_{22}^{\varepsilon 0} & 0 \\ \chi_{13}^{\varepsilon 0} & 0 & \chi_{33}^{\varepsilon 0} \end{pmatrix}. \tag{2.3}$$

In the paraelectric phase, all coefficients $e_{ij}^{0} \equiv 0$.

Other terms in (2.1) describe the pseudospin part of the Hamiltonian. In particular, the second term in (2.1) is the Hamiltonian of short-range interactions:

$$\hat{H}_{\text{short}} = -2\sum_{qq'}\left(w_1\frac{\sigma_{q1}}{2}\frac{\sigma_{q2}}{2} + w_2\frac{\sigma_{q3}}{2}\frac{\sigma_{q4}}{2}\right) \times \left(\delta_{\mathbf{R}_q\mathbf{R}_{q'}} + \delta_{\mathbf{R}_q+\mathbf{R}_{\mathbf{c}},\mathbf{R}_{q'}}\right). \tag{2.4}$$

In (2.4), σ_{qf} is the z-component of the pseudospin operator that describes the state of the f-th bond (f = 1, 2, 3, 4) in the q-th cell. The first Kronecker delta corresponds to the interaction between protons in the chains near the tetrahedra HPO_3 of type "I" (see Fig. 1), while the second one near the tetrahedra HPO_3 of type "II", $\mathbf{R}_{\mathbf{c}}$ is the lattice vector along OZ-axis. The contributions into the energy of interactions between the protons near tetrahedra of different types, as well as the mean

values of the pseudospins $\eta_f = \langle\sigma_{qf}\rangle$, which are related to the tetrahedra of different types, are identical.

Parameters w_1, w_2, which describe the short-range interactions within the chains, are expanded linearly into series over strains ε_j:

$$w_{1,2} = w^0 + \sum_l \delta_l\varepsilon_l \pm \delta_4\varepsilon_4 \pm \delta_6\varepsilon_6, \quad (l = 1, 2, 3, 5). \quad (2.5)$$

The third term in (2.1) describes the long-range dipole-dipole interactions and indirect (through the lattice vibrations) interactions between protons which are taken into account in the mean field approximation:

$$\hat{H}_{\rm long} = \frac{1}{2}\sum_{\substack{qq'\\ff'}} J_{ff'}(qq')\frac{\langle\sigma_{qf}\rangle}{2}\frac{\langle\sigma_{q'f'}\rangle}{2} - \sum_{\substack{qq'\\ff'}} J_{ff'}(qq')\frac{\langle\sigma_{q'f'}\rangle}{2}\frac{\sigma_{qf}}{2}. \quad (2.6)$$

Fourier transforms of interaction constants $J_{ff'} = \sum_{q'} J_{ff'}(qq')$ at $\mathbf{k} = 0$ are linearly expanded over strains ε_j:

$$J_{\frac{11}{33}} = J^0_{11} + \sum_l \psi_{11l}\varepsilon_l \pm \psi_{114}\varepsilon_4 \pm \psi_{116}\varepsilon_6, J_{13} = J^0_{13} + \sum_l \psi_{13l}\varepsilon_l + \psi_{134}\varepsilon_4 + \psi_{136}\varepsilon_6,$$

$$J_{\frac{12}{34}} = J^0_{12} + \sum_l \psi_{12l}\varepsilon_l \pm \psi_{124}\varepsilon_4 \pm \psi_{126}\varepsilon_6, J_{\frac{14}{23}} = J^0_{14} + \sum_l \psi_{14l}\varepsilon_l \pm \psi_{144}\varepsilon_4 \pm \psi_{146}\varepsilon_6, \quad (2.7)$$

$$J_{\frac{22}{44}} = J^0_{22} + \sum_l \psi_{22l}\varepsilon_l \pm \psi_{224}\varepsilon_4 \pm \psi_{226}\varepsilon_6, J_{24} = J^0_{24} + \sum_l \psi_{24l}\varepsilon_l + \psi_{244}\varepsilon_4 + \psi_{246}\varepsilon_6.$$

In model [5], there is sign "+" instead of "±" in expressions (2.5) and (2.7), that is $w_1 = w_2$, $J_{11} = J_{33}$, $J_{12} = J_{34}$, $J_{14} = J_{23}$, $J_{22} = J_{44}$.

As a result, (2.6) can be written as:

$$\hat{H}_{\rm long} = NH^0 - \sum_q \sum_{f=1}^{4} \mathcal{H}_f \frac{\sigma_{qf}}{2}, \quad (2.8)$$

where

$$H^0 = \sum_{f,f'=1}^{4} \frac{1}{8} J_{ff'}\eta_f\eta_{f'}, \quad \mathcal{H}_f = \sum_{f'=1}^{4} \frac{1}{2} J_{ff'}\eta_{f'}. \quad (2.9)$$

The fourth term in (2.1) describes the interactions of pseudospins with the external electric field:

$$\hat{H}_E = -\sum_{qf} \boldsymbol{\mu}_f \mathbf{E} \frac{\sigma_{qf}}{2}. \quad (2.10)$$

Here, $\boldsymbol{\mu}_1 = (\mu^x_{13}, \mu^y_{13}, \mu^z_{13})$, $\boldsymbol{\mu}_3 = (-\mu^x_{13}, \mu^y_{13}, -\mu^z_{13})$, $\boldsymbol{\mu}_2 = (-\mu^x_{24}, -\mu^y_{24}, \mu^z_{24})$, $\boldsymbol{\mu}_4 = (\mu^x_{24}, -\mu^y_{24}, -\mu^z_{24})$ are the effective dipole moments per one pseudospin.

In [7], using Hamiltonian (2.1) and the two-particle cluster approximation, the thermodynamic potential of GPI was obtained in the presence of mechanical stresses and electric fields. On the basis of this thermodynamic potential, the expressions for the dielectric, piezoelectric and thermal characteristics were derived for any direction of the stress or field. In the present paper, we use the expressions obtained in [7] for the calculation of the simultaneous effect of the shear stress σ_5 or σ_6 together with the electric field E_3 on the thermodynamic characteristics of GPI. We do not show the explicit expressions for these characteristics in the present paper because of their complicated nature.

III. THE RESULTS OF NUMERICAL CALCULATIONS

For the numerical calculation of the dielectric and piezoelectric characteristics of GPI, we have used the parameters determined in [7] and earlier in [5] from the condition of agreement of the calculated characteristics with experimental data. They are enumerated below.

- The parameter of the short-range interactions $w_0/k_{\rm B}$=800 K (820 K in [5]);

- The parameters of the long-range interactions appear in the expressions obtained in [5, 7] in the form of such combinations $\nu^{0\pm}_1 = \frac{1}{4}(J^0_{11} \pm J^0_{13})$, $\nu^{0\pm}_2 = \frac{1}{4}(J^0_{12} \pm J^0_{14})$, $\nu^{0\pm}_3 = \frac{1}{4}(J^0_{22} \pm J^0_{24})$; they are equal to: $\tilde{\nu}^{0+}_1 = \tilde{\nu}^{0+}_2 = \tilde{\nu}^{0+}_3$=3.065 K (2.643 K in [5]), $\tilde{\nu}^{0-}_1 = \tilde{\nu}^{0-}_2 = \tilde{\nu}^{0-}_3$=0.05K (0.2K in [5]), where $\tilde{\nu}^{0\pm}_f = \nu^{0\pm}_f/k_{\rm B}$.

- The optimal values of the deformational potentials: $\tilde{\delta}_1$=500 K, $\tilde{\delta}_2$=600 K, $\tilde{\delta}_3$=500 K, $\tilde{\delta}_4$=150 K, $\tilde{\delta}_5$=100 K, $\tilde{\delta}_6$=150 K; $\tilde{\delta}_i = \delta_i/k_{\rm B}$;
the parameters $\psi_{ii'j}$ also appear in the expressions obtained in [5, 7] in the form of combinations $\psi^{\pm}_{1j} = \frac{1}{4}(\psi_{11j} \pm \psi_{13j})$, $\psi^{\pm}_{2j} = \frac{1}{4}(\psi_{12j} \pm \psi_{14j})$, $\psi^{\pm}_{3j} = \frac{1}{4}(\psi_{22j} \pm \psi_{24j})$. These combinations are equal to: $\tilde{\psi}^{+}_{f1}$ = 93.6 K, $\tilde{\psi}^{+}_{f2}$ = 252.5 K, $\tilde{\psi}^{+}_{f3}$ = 110.7 K, $\tilde{\psi}^{+}_{f4} = \tilde{\psi}^{+}_{f6} = \tilde{\psi}^{-}_{f4} = \tilde{\psi}^{-}_{f6}$=79.5 K, $\tilde{\psi}^{+}_{f5}$ = 22.7 K,

$\tilde{\psi}^{-}_{f1}$=$\tilde{\psi}^{-}_{f2}$=$\tilde{\psi}^{-}_{f3}$=$\tilde{\psi}^{-}_{f5}$=0 K, where $\tilde{\psi}^{\pm}_{fi}$ =$\psi^{\pm}_{fi}/k_{\rm B}$. In [5] the parameters $\tilde{\psi}^{\pm}_{fi}$ were: $\tilde{\psi}^{+}_{f1}$ = 87.9 K, $\tilde{\psi}^{+}_{f2}$ = 237.0 K, $\tilde{\psi}^{+}_{f3}$ = 103.8 K, $\tilde{\psi}^{+}_{f4}$ = 149.1 K, $\tilde{\psi}^{+}_{f5}$ = 21.3 K, $\tilde{\psi}^{+}_{f6}$ = 143.8 K, $\tilde{\psi}^{-}_{fi}$=0 K.

- The components of effective dipole moments in the paraelectric phase are equal to μ^{x}_{13}=0.4·10^{-18} esu·cm; μ^{y}_{13}=4.05·10^{-18} esu·cm (4.02·10^{-18} esu·cm in [5]); μ^{z}_{13}=4.2·10^{-18} esu·cm (4.3·10^{-18} esu·cm in [5]); μ^{x}_{24}=2.3·10^{-18} esu·cm; μ^{y}_{24}=3.0·10^{-18} esu·cm; μ^{z}_{24}=2.2·10^{-18} esu·cm. In the ferroelectric phase, the y-component of the first dipole moment is $\mu^{y}_{13\rm ferro} = 3.82\cdot10^{-18}$ esu·cm; the other components are such as in the paraelectric phase.

- The volume of the primitive cell of GPI is v = 0.601·10^{-21} cm^3.

- The "seed" coefficients of piezoelectric stress e^{0}_{ij}, "seed" dielectric susceptibilities $\chi^{\varepsilon 0}_{ij}$ and "seed" elastic constants c^{E0}_{ij} are obtained as follows: e^{0}_{ij} = 0.0$\frac{\rm esu}{\rm cm^2}$;

$\chi^{\varepsilon 0}_{11}$ = 0.1, $\chi^{\varepsilon 0}_{22}$= 0.403, $\chi^{\varepsilon 0}_{33}$ = 0.5, $\chi^{\varepsilon 0}_{31}$ = 0.0;

c^{0E}_{11} = 269.1 kbar, c^{E0}_{12} = 145 kbar,

c^{E0}_{13} = 116.4 kbar, c^{E0}_{15} = 39.1 kbar,

c^{E0}_{22} = (649.9 − 0.4($T - T_c$)) kbar,

c^{E0}_{23} = 203.8 kbar, c^{E0}_{25} = 56.4 kbar,

c^{E0}_{33} = 244.1 kbar, c^{E0}_{35} = −28.4 kbar,

c^{E0}_{55} = 85.4 kbar, c^{E0}_{44} = 153.1 kbar,

c^{E0}_{46} = −11 kbar, c^{E0}_{66} = 118.8 kbar.

Now, let us dwell upon the obtained results. Figure 2 presents the temperature dependences of spontaneous polarization P_2, inverse longitudinal dielectric permittivity ε^{-1}_{22}, transverse permittivities ε_{11} and ε_{33}, molar heat capacity C_p, piezoelectric coefficients e_{2i}, d_{2i}, h_{2i} and g_{2i} of the GPI crystal calculated in [5] (dash-dotted lines), as well as corresponding temperature dependences calculated later in [7] taking into account the change of symmetry in the presence of the shear strains ε_4 or ε_6 (solid lines).

As one can see from Fig. 2, taking into account the change of symmetry and the corresponding correction of the theory parameters have weakly influenced the thermodynamic characteristics of the GPI crystal in the absence of any stresses and fields. The results of the investigation into the effects of the hydrostatic and uniaxial pressure on the thermodynamic characteristics of GPI, which are calculated using the earlier parameters [12,13] and the corrected parameters [7], do not much differ either.

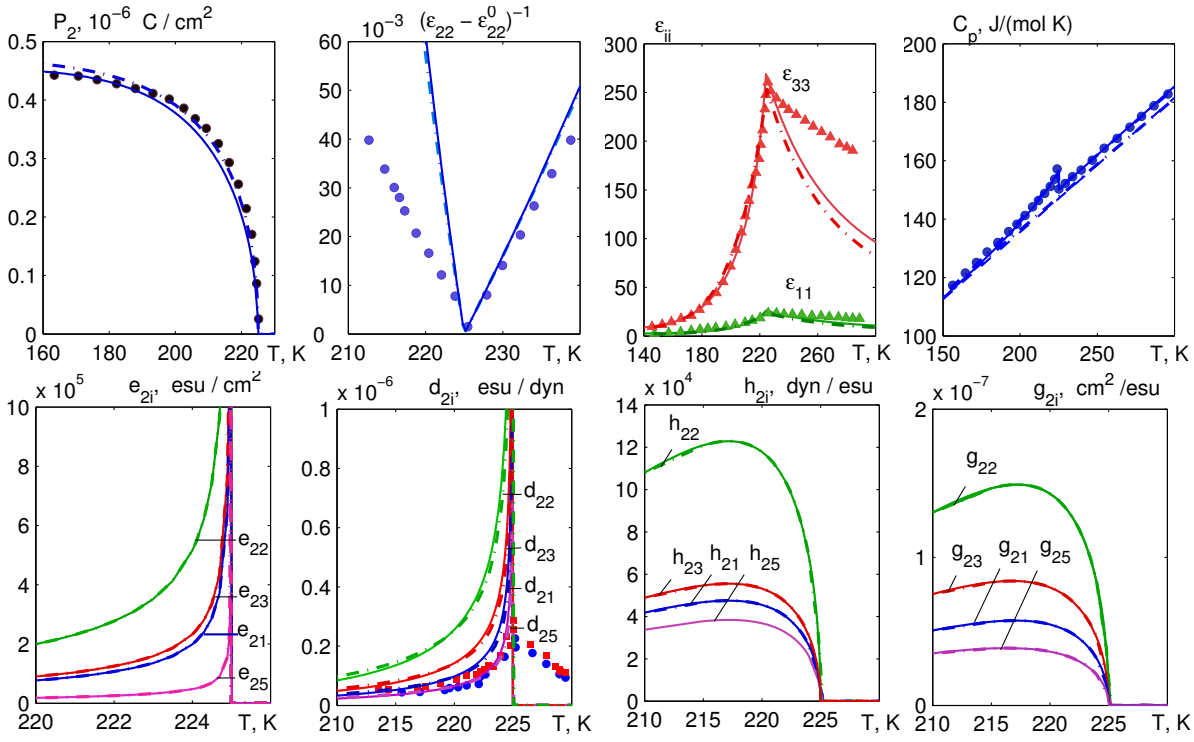

Fig. 2. (Color online). The temperature dependences of spontaneous polarization P_2 (● – [8]), inverse longitudinal dielectric permittivity ε^{-1}_{22} (● – [9]), transverse permittivities ε_{11}, ε_{33} (▲, ▲ – [1]), molar heat capacity C_p (● – [10]), piezoelectric coefficients e_{2i}, d_{2i} (d_{21} – ● [11], d_{23} – ● [11]), h_{2i}, g_{2i} of GPI crystal.

Now let us consider how to change the thermodynamic characteristics of the GPI crystal at the simultaneous application of the shear stress σ_5 or σ_6 and the electric field E_3. It should be noted that experimental data for ε_{22} obtained by different authors slightly differ from each other (see [5]). I is quite likely that this is connected with the different quality of the samples. In our model, this disagreement means different effective dipole moments μ_{13}^y in different samples. We assume that there can exist a sample with the same μ_{13}^y in the ferro- and paraelectric phases. Therefore, for the sake of simplicity, hereinafter we consider a case of the GPI sample with the same value of the effective dipole moment in the paraelectric and ferroelectric phase $\mu_{13\text{ferro}}^y$=$\mu_{13\text{para}}^y$=$3.82{\cdot}10^{-18}$ esu·cm.

Also we must note that in all further figures the main number 5 or 6 means the direction of the applied stress (σ_5 or σ_6, respectively), the upper index shows the value of the stress (kbar), and the lower index shows the value of the electric field strength (MV/m). For example, the notation 5_4^{-2} means the shear stress $\sigma_5 = -2$ kbar and electric field $E_3 = 4$ MV/m applied simultaneously.

Figure 3 shows the dependences of the phase transition temperature T_c in the GPI crystal on the electric field E_3 at different values of the shear stress σ_5.

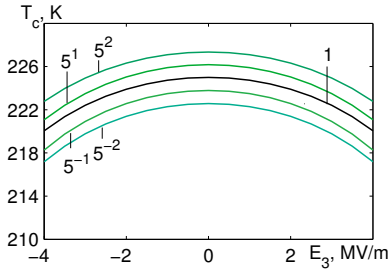

Fig. 3. The dependences of the phase transition temperature T_c in GPI crystal on the electric field E_3 at different values of the shear stress σ_5. Curve 1 corresponds to the case of $\sigma_j = 0$, another curves correspond to the stresses $\sigma_5 = \pm1, \pm2$ kbar.

In the absence of the stress, temperature T_c depends on field E_3 by the law $T_c(E_3) \sim -E_3^2$ (curve 1 in Fig. 3). On the other hand, at zero field, temperature T_c linearly increases with stress σ_5 because of the strengthening of the interactions between pseudospins under this stress (see [7]). Since stress σ_5 does not change the symmetry of the crystal, the curve $T_c(E_3)$ qualitatively does not change under this stress, but only shifts in temperature (Fig. 3, curves $5^{\pm1}$, $5^{\pm2}$ at $\sigma_5 = \pm1, \pm2$ kbar, respectively).

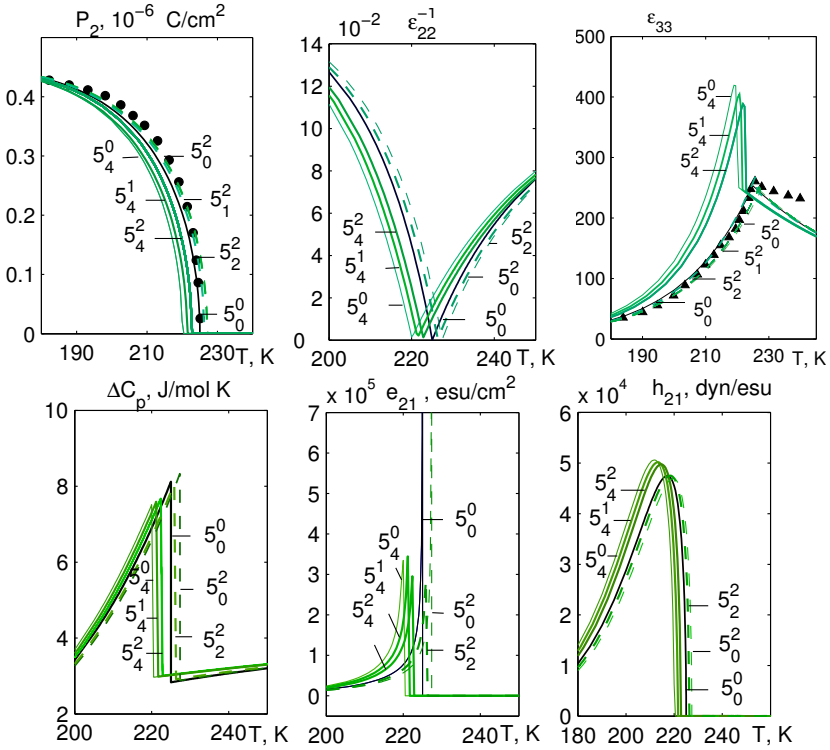

Fig. 4. The temperature dependences of polarization P_2 (• are taken from [8]), inverse longitudinal dielectric permittivity ε_{22}^{-1}, transverse dielectric permittivity ε_{33} (▲ – [1]), proton contribution to molar heat capacity ΔC_p, longitudinal piezoelectric coefficients e_{21}, h_{21} of GPI crystal at different values of the stress σ_5 and the electric field E_3.

The temperature dependences of the thermodynamic characteristics at different values of stress σ_5 and electric field E_3 are presented in Figs. 4 and 5. On these figures curves 5_0^0 correspond to the case of a zero stress and field. In the special case of a zero stress but a nonzero field E_3 (curves 5_4^0 at $\sigma_5 = 0$ kbar and $E_3 = 4$ MV/m), the curves

of temperature dependences are shifted to lower temperatures in relation to curves 5^0_0. Besides, as one can see from Fig. 4, permittivity ε_{33} in the ferroelectric phase significantly increases in the presence of field E_3. As was shown in [6], the decrease of T_c and increase in ε_{33} in the ferroelectric phase are connected with the partial disordering in the chain "B" (Fig. 1) under the action of field E_3. One more peculiarity is the change of sign of the transverse piezoelectric coefficients e_{1j}, e_{3j}, h_{1j} and h_{3j} near T_c (see Fig. 5) in field E_3, which is connected with almost complete disordering of protons in the chain "B" near T_c, as was shown in [14].

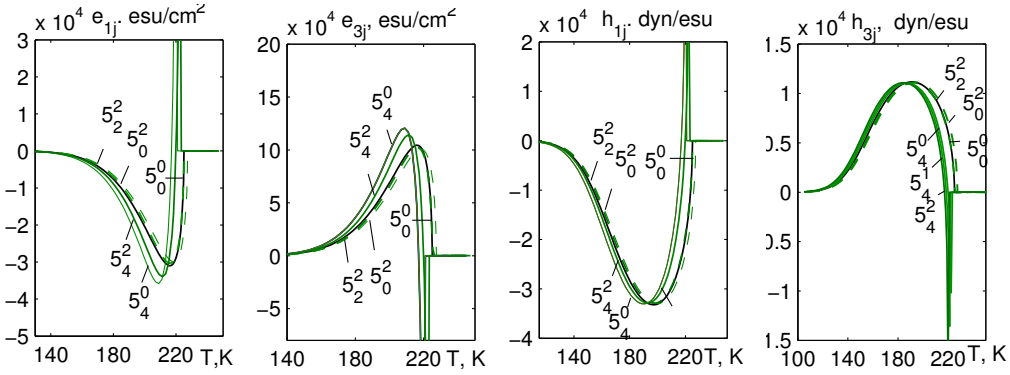

Fig. 5. The temperature dependences of transverse piezoelectric coefficients $e_{1j} = e_{14} = e_{16}$, $e_{3j} = e_{34} = e_{36}$, $h_{1j} = h_{14} = h_{16}$ and $h_{3j} = h_{34} = h_{36}$ of GPI crystal at different values of the stress σ_5 and the electric field E_3.

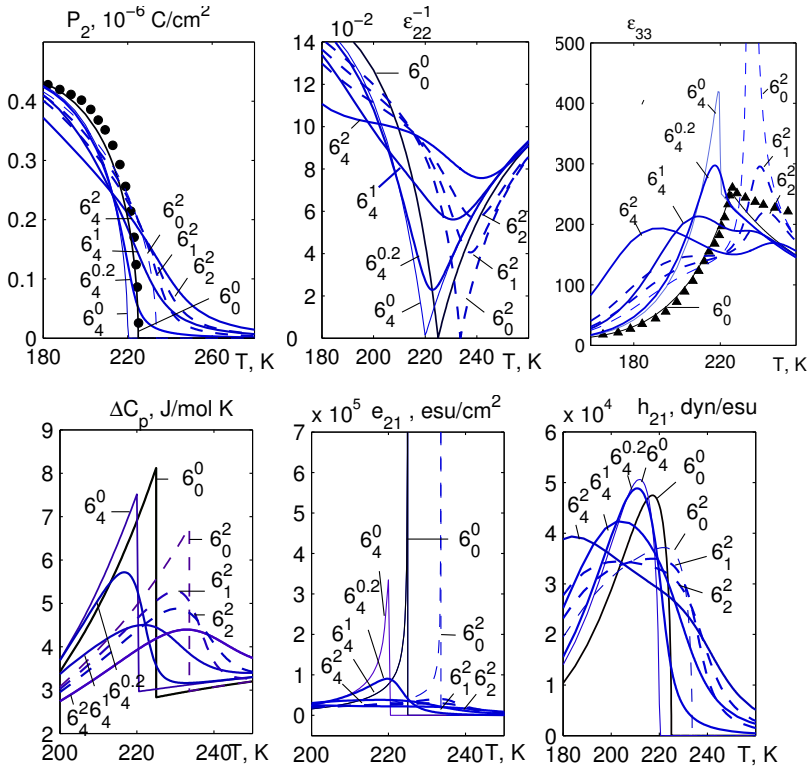

Fig. 6. The temperature dependences of polarization P_2 (• – [8]), inverse longitudinal dielectric permittivity ε_{22}^{-1}, transverse dielectric permittivity ε_{33} (▲ – [1]), proton contribution to molar heat capacity ΔC_p, longitudinal piezoelectric coefficients e_{21}, h_{21} of GPI crystal at different values of the stress σ_6 and the electric field E_3.

Stress σ_5 at the constant field E_3 leads to a shift of the curves of the temperature dependences of the abovementioned thermodynamic characteristics to higher temperatures. That is, curves 5^2_0 (2 kbar,0 MV/m) are shifted to higher temperatures in relation to curves 5^0_0 (0 kbar,0 MV/m); curves 5^2_4 are shifted in relation to 5^0_4 and so on.

In the case of the application of the shear stress σ_6 in a zero field (curves 6^2_0 in all the figures), the symmetry of the crystal reduces, and the two sublattices (the chains "A" and "B") become nonequivalent (see [7]). As a result, the interactions between pseudospins in chain "A" become stronger, but in chain "B" they become weaker. Strengthening of interactions in a sublattice at some

value of stress σ_6 causes a phase transition to the ferroelectric phase and increases temperature T_c. Therefore, curves $P_2(T)$, $\varepsilon_{22}(T)$, $e_{21}(T)$, $h_{21}(T)$, $\Delta C_p(T)$ shift to higher temperatures (Fig. 6). Since chains "A" and "B" become nonequivalent, then the polarizations of both sublattices in the XZ plane do not compensate each other, similarly as in ferrimagnets. As a result, there appear the components of spontaneous polarization P_1 and P_3 (Fig. 7) in the XZ plane, and the transverse permittivity $\varepsilon_{33}(T)$ (Fig. 6, curve 6_0^2) looks like a longitudinal component of dielectric permittivity.

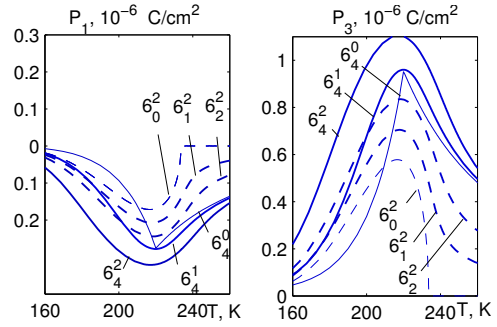

Fig. 7. The temperature dependences of polarizations P_1 and P_3 of GPI crystal at different values of the stress σ_6 and the electric field E_3.

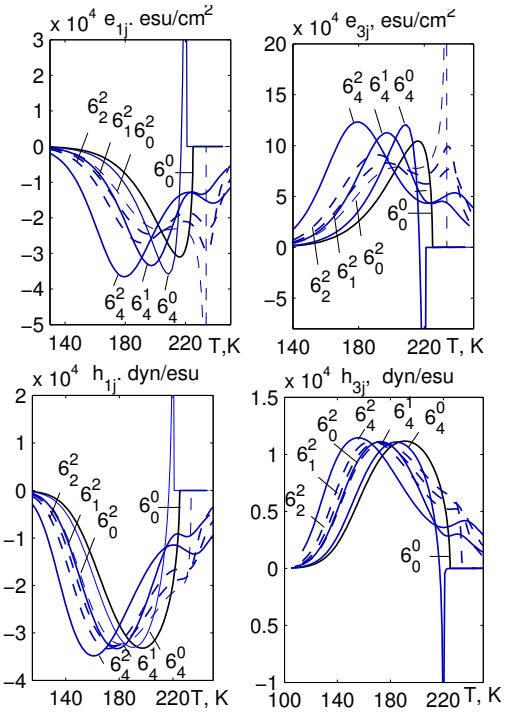

Fig. 8. The temperature dependences of piezoelectric coefficients e_{1j}, e_{3j}, h_{1j} i h_{3j} of GPI crystal at different values of the stress σ_6 and the electric fields E_3.

It is necessary to note that in the presence of stress σ_6 and in a zero field, components $P_1 \neq 0$ and $P_3 \neq 0$ only in the ferroelectric phase (Fig. 7, curves 6_0^2), whereas in the other special case, $\sigma_6 = 0$ and $E_3 \neq 0$, components $P_1 \neq 0$ and $P_3 \neq 0$ at all temperatures (curves 6_4^0).

As one can see from Fig. 8 (curves 6_0^2), the piezoelectric coefficients $e_{1j}(T)$, $e_{3j}(T)$ tend to infinity in point T_c. This is because under a nonzero stress σ_6 the small changes in strains $d\varepsilon_4$, $d\varepsilon_6$ are accompanied by a change in temperature dT_c and by a shift of curves $P_1(T)$ and $P_3(T)$ to higher temperatures. Inasmuch as $dP_i/dT \to \infty$ near the phase transition temperature, then $dP_i/d\varepsilon_4 \to \infty$, $dP_i/d\varepsilon_6 \to \infty$.

Since all the components $P_\alpha \neq 0$ under stress σ_6 in the ferroelectric phase, field E_3, which is applied additionally to stress σ_6, contains a component parallel to the total polarization (the longitudinal component $\mathbf{E}_3^* \parallel \mathbf{P}$). This longitudinal component leads to the smearing of the phase transition (curves 6_1^2, 6_2^2, 6_4^1, 6_4^2, $6_4^{0.2}$).

IV. CONCLUSIONS

The reducing of the symmetry of interactions under shear stresses ε_4 and ε_6 practically does not affect the components of the spontaneous polarization vector, dielectric permittivity tensor, longitudinal piezoelectric coefficients, elastic constants, and molar heat capacity. However, it allows to calculate also the transverse piezoelectric coefficients.

Dielectric properties of GPI depend on the way of the application of mechanical stresses and fields. The application of only the electric field E_3 in the absence of mechanical stresses decreases temperature T_c, increases permittivity ε_{33} in the ferroelectric phase, and also induces the components of polarization P_1 and P_3 in the whole temperature range. The shear stress σ_5, which is applied additionally to field E_3, qualitatively does not change the temperature dependences of thermodynamic characteristics, but only linearly increases the phase transition temperature.

The application of only the shear stress σ_6 to the crystal reduces the symmetry of the crystal, and chains "A" and "B" become nonequivalent. Consequently, in the ferroelectric phase, besides component P_2, the components of polarization P_1 and P_3 appear in the XZ plane. That is, the total spontaneous polarization vector is nonperpendicular to the OZ axis. Therefore, field E_3, which is applied additionally to stress σ_6, contains the component parallel to the total polarization (the longitudinal component). This longitudinal component leads to the smearing of the phase transition.

[1] S. Dacko, Z. Czapla, J. Baran, M. Drozd, Phys. Lett. A **223**, 217 (1996); https://doi.org/10.1016/S0375-9601(96)00698-6.

[2] I. Stasyuk, Z. Czapla, S. Dacko, O. Velychko, Condens. Matter Phys. **6**, 483 (2003); https://doi.org/10.5488/CMP.6.3.483.

[3] I. Stasyuk, Z. Czapla, S. Dacko, O. Velychko, J. Phys. Condens. Matter. **16**, 1963 (2004); https://doi.org/10.1088/0953-8984/16/12/006.
[4] I. Stasyuk, O. Velychko, Ferroelectrics **300**, 121 (2004); https://doi.org/10.1080/00150190490443622.
[5] I. R. Zachek, Ya. Shchur, R. R. Levitskii, A. S. Vdovych, Physica B **520**, 164 (2017); https://doi.org/10.1016/j.physb.2017.06.013.
[6] I. R. Zachek, R. R. Levitskii, A. S. Vdovych, I. V. Stasyuk, Condens. Matter Phys. **20**, 23706 (2017); https://doi.org/10.5488/CMP.20.23706.
[7] I. R. Zachek, R. R. Levitskii, A. S.Vdovych, Condens. Matter Phys. **21**, 33702 (2018); https://doi.org/10.5488/CMP.21.33702.
[8] J. Nayeem *et al.*, Ferroelectrics, **332**, 13 (2006); https://doi.org/10.1080/00150190500309064.
[9] J. Nayeem, H. Wakabayashi, T. Kikuta, T. Yamazaki, N. Nakatani, Ferroelectrics **269**, 153 (2002); https://doi.org/10.1080/713716051.
[10] F. Shikanai, J. Hatori, M. Komukae, Z. Czapla, T. Osaka, J. Phys. Soc. Jpn. **73**, 1812 (2004); https://doi.org/10.1143/JPSJ.73.1812.
[11] M. Wiesner, Phys. Status Solidi (b) **238**, 68 (2003); https://doi.org/10.1002/pssb.200301750.
[12] I. R. Zachek, R. R. Levitskii, A. S. Vdovych, Condens. Matter Phys. **20**, 43707, (2017), https://doi.org/10.5488/CMP.20.43707.
[13] I. R. Zachek, R. R. Levitskii, A. S. Vdovych. J. Phys. Stud. **21**, 1704, (2017).
[14] A. S. Vdovych, I. R. Zachek, R. R. Levitskii, Math. Model. Comput. **5**, 242, (2018); https://doi.org/10.23939/mmc2018.02.242.

ВПЛИВ НАПРУГ σ_5, σ_6 ТА ЕЛЕКТРИЧНОГО ПОЛЯ E_3 НА ТЕРМОДИНАМІЧНІ ХАРАКТЕРИСТИКИ СЕГНЕТОЕЛЕКТРИКА GPI

А. С. Вдович[1], Р. Р. Левицький[1], І. Р. Зачек[2]
[1] *Інститут фізики конденсованих систем НАН України*
вул. Свєнціцького, 1, Львів, 79011, Україна
[2] *Національний університет "Львівська політехніка"*
вул. С. Бандери 12, 79013, Львів, Україна

Для дослідження ефектів, що виникають під дією зсувних напруг σ_5, σ_6 та електричного поля E_3, використано модифіковану модель сегнетоелектрика фосфіту гліцину (GPI) через врахування п'єзоелектричного зв'язку структурних елементів, які впорядковуються, з деформаціями ε_j. В наближенні двочастинкового кластера розраховано вектори поляризації та компоненти тензора статичної діелектричної проникності механічно затиснутого кристала, їхні п'єзоелектричні та теплові характеристики. Досліджено одночасну дію напруги σ_5 і поля E_3, а також напруги σ_6 і поля E_3 на фазовий перехід та фізичні характеристики кристала.